

# The ${}^8\text{Li}(d,p){}^9\text{Li}$ Reaction and the Astrophysical ${}^8\text{Li}(n,\gamma){}^9\text{Li}$ Reaction Rate

Z. H. Li,\* W. P. Liu, X. X. Bai, B. Guo, G. Lian, S. Q. Yan, B. X.

Wang, S. Zeng, Y. Lu, J. Su, Y. S. Chen, K. S. Wu, and N. C. Shu

*China Institute of Atomic Energy, P. O. Box 275(46), Beijing 102 413, P. R. China*

T. Kajino

*National Astronomical Observatory of Japan, Mitaka, Tokyo 181-8588, Japan;*

*Department of Astronomy, University of Tokyo, Bunkyo-ku, Tokyo 113-0033 Japan*

(Dated: October 20, 2018)

## Abstract

The  ${}^8\text{Li}(n,\gamma){}^9\text{Li}$  reaction plays an important role in both the r-process nucleosynthesis and the inhomogeneous big bang models, its direct capture rates can be extracted from the  ${}^8\text{Li}(d,p){}^9\text{Li}$  reaction, indirectly. We have measured the angular distribution of the  ${}^8\text{Li}(d,p){}^9\text{Li}_{\text{g.s.}}$  reaction at  $E_{\text{c.m.}} = 7.8$  MeV in inverse kinematics using coincidence detection of  ${}^9\text{Li}$  and recoil proton, for the first time. Based on Distorted Wave Born Approximation (DWBA) analysis, the  ${}^8\text{Li}(d,p){}^9\text{Li}_{\text{g.s.}}$  cross section was determined to be  $7.9 \pm 2.0$  mb. The single particle spectroscopic factor,  $S_{1,3/2}$ , for the ground state of  ${}^9\text{Li} = {}^8\text{Li} \otimes n$  was derived to be  $0.68 \pm 0.14$ , and then used to calculate the direct capture cross sections for the  ${}^8\text{Li}(n,\gamma){}^9\text{Li}_{\text{g.s.}}$  reaction at energies of astrophysical interest. The astrophysical  ${}^8\text{Li}(n,\gamma){}^9\text{Li}_{\text{g.s.}}$  reaction rate for the direct capture was found to be  $3970 \pm 950$   $\text{cm}^3\text{mole}^{-1}\text{s}^{-1}$  at  $T_9 = 1$ . This presents the first experimental constraint for the  ${}^8\text{Li}(n,\gamma){}^9\text{Li}$  reaction rates of astrophysical relevance.

PACS numbers: 25.60.Je, 21.10.Jv, 25.40.Lw, 26.35.+c

---

\*Electronic address: zhli@ciae.ac.cn

The  ${}^8\text{Li}(n, \gamma){}^9\text{Li}$  reaction has attracted much attention in the recent years because of its importance in astrophysics. In the explosive neutron-rich environments, the stability gap at mass number  $A = 8$  can be bridged with reactions involving the unstable nucleus  ${}^8\text{Li}$  to synthesize  $A > 8$  nuclides. Type II supernovae and inhomogeneous big bang nucleosynthesis are thought to be the astrophysical sites for such nucleosynthetic processes.

In the recently developed scenario of the r-process nucleosynthesis occurring in the circumstances of type II supernovae [1, 2], all preexisting nuclei, in the region between the nascent neutron star and the shock front, are believed to have been photo-disintegrated to protons and neutrons at the initial high temperature. With the descent of temperature, they recombine mostly under nuclear statistical equilibrium, leading to the production of seed nuclei for r-process. When a high  $\alpha$ -particle abundance forms, the main reaction chain is initiated by  ${}^4\text{He}(\alpha n, \gamma){}^9\text{Be}(\alpha, n){}^{12}\text{C}$ . After  $\alpha$ -rich freezeout, however,  ${}^4\text{He}(t, \gamma){}^7\text{Li}(n, \gamma){}^8\text{Li}(\alpha, n){}^{11}\text{B}$  becomes one of the active reaction chains to produce seed nuclei. In this phase, the  ${}^8\text{Li}(n, \gamma){}^9\text{Li}$  reaction, that leads to the production of  ${}^9\text{Be}$  via the  ${}^9\text{Li}$   $\beta$ -decay, is in competition with the  ${}^8\text{Li}(\alpha, n){}^{11}\text{B}$  reaction. The competition determines which reaction path is taken. This reaction also competes with the  ${}^8\text{Li}$   $\beta$ -decay. Depending on the rate,  ${}^8\text{Li}(n, \gamma){}^9\text{Li}$  may influence the abundances of seed nuclei to some extent. Recently, binary neutron star mergers have been proposed as the possible alternative sites for the r-process [3], in which similar situation is also found.

The inhomogeneous big bang models [4] predict relatively higher abundances of  $A > 8$  nuclides than the standard model does. An unconvincing agreement [5] between the observed primordial abundances and predicted ones with the standard model may be a hint for the need of inhomogeneous models, in which  ${}^7\text{Li}(n, \gamma){}^8\text{Li}(\alpha, n){}^{11}\text{B}$  are generally thought to be the major reaction chain forming heavier nuclei. However, it has been found that  ${}^7\text{Li}(n, \gamma){}^8\text{Li}(n, \gamma){}^9\text{Li}(\alpha, n){}^{12}\text{B}$  may be even more important [6]. Thus the  ${}^8\text{Li}(n, \gamma){}^9\text{Li}$  reaction affects not only the reaction path to  $A > 8$  isotopes but also the abundances of Li, Be, B and C.

Considerable effort has been devoted to experimentally determining the  ${}^8\text{Li}(\alpha, n){}^{11}\text{B}$  cross section as described in Ref. [7] and references therein. However, a large uncertainty still remains for the  ${}^8\text{Li}(n, \gamma){}^9\text{Li}$  cross section. There were some microscopic and systematic calculations of this reaction that deviated by order of magnitude [6, 8, 9, 10, 11, 12]. Direct measurement of the  ${}^8\text{Li}(n, \gamma){}^9\text{Li}$  reaction is impossible because no neutron target exists and

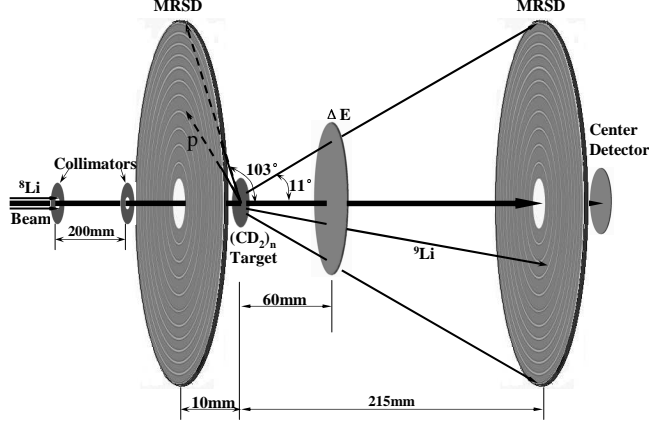


FIG. 1: Schematic layout of the experimental setup.

the half life of  ${}^8\text{Li}$  is too short (838 ms) as a target. The only experimental information was obtained from two Coulomb dissociation measurements [13, 14] that presented the different upper limits. It is therefore highly needed to measure the  ${}^8\text{Li}(n, \gamma){}^9\text{Li}$  cross section through an independent approach. It is a practicable method to extract the direct capture cross section for the  ${}^8\text{Li}(n, \gamma){}^9\text{Li}$  reaction using the direct capture model [15, 16] and spectroscopic factor which can be deduced from the angular distribution of the transfer reaction  ${}^8\text{Li}(d, p){}^9\text{Li}$ .

Up to now, the only measurement of the  ${}^8\text{Li}(d, p){}^9\text{Li}$  reaction was performed in 1990's [17], in which an upper limit of cross section was presented though no  ${}^9\text{Li}$  events were detected. In present work, we measured the angular distribution of the  ${}^8\text{Li}(d, p){}^9\text{Li}_{\text{g.s.}}$  ( $Q = 1.839$  MeV) reaction at  $E_{\text{c.m.}} = 7.8$  MeV in inverse kinematics and derived the  ${}^8\text{Li}(n, \gamma){}^9\text{Li}_{\text{g.s.}}$  direct capture cross sections at energies of astrophysical interest.

The experiment was carried out using the secondary beam facility GIRAFFE [18] of the HI-13 tandem accelerator, Beijing. A 44 MeV  ${}^7\text{Li}$  primary beam from the tandem impinged on a 4.8 cm long deuterium gas cell at a pressure of 1.6 atm. The front and rear windows of the gas cell were Havar foils, each in thickness of  $1.9$  mg/cm<sup>2</sup>. The  ${}^8\text{Li}$  ions were produced via the  ${}^2\text{H}({}^7\text{Li}, {}^8\text{Li}){}^1\text{H}$  reaction. After the magnetic separation and focus with a dipole and a quadrupole doublet, the 39 MeV  ${}^8\text{Li}$  secondary beam was delivered. Typical purity of the  ${}^8\text{Li}$  beam was about 80%, the main contaminants were  ${}^7\text{Li}$  ions out of Rutherford scattering of the primary beam in the gas cell windows as well as beam tube. The  ${}^8\text{Li}$  beam was then collimated with two apertures in diameter of 3 mm and directed onto a  $(\text{CD}_2)_n$  target in thickness of  $1.5$  mg/cm<sup>2</sup> to study the  ${}^2\text{H}({}^8\text{Li}, {}^9\text{Li}){}^1\text{H}$  reaction, the typical beam intensity on

the target was approximately 1000 pps. The beam energy spread on the target was 0.52 MeV FWHM for long-term measurement, and the beam angular divergence was about  $\pm 0.3^\circ$ . A carbon target in thickness of 1.8 mg/cm<sup>2</sup> served as the background measurement.

The experimental setup is shown in Fig. 1. Two 300  $\mu\text{m}$  thick Multi-Ring Semiconductor Detectors (MRSDs) with center holes were used. The upstream one aimed at detection of the recoil protons, and the downstream one backed by an independent 300  $\mu\text{m}$  thick silicon detector placed at the center hole served as a residue energy  $E_r$  detector which composed a  $\Delta E - E_r$  counter telescope together with a 21.7  $\mu\text{m}$  thick silicon  $\Delta E$  detector. Such a detector configuration covered the laboratory angular ranges from  $0^\circ$  to  $11^\circ$  (greater than the maximum  $\theta_{\text{lab}}$  of  $^9\text{Li}$ ,  $10.7^\circ$ ) and from  $103^\circ$  to  $170^\circ$  respectively. For coincidence measurement, the detectable angular range of  $^9\text{Li}$  in center of mass system was from  $10^\circ$  to  $50^\circ$ . This setup also facilitated to precisely determine the accumulated quantity of incident  $^8\text{Li}$  because the  $^8\text{Li}$  themselves were recorded by the counter telescope simultaneously.

The accumulated quantity of incident  $^8\text{Li}$  for the  $(\text{CD}_2)_n$  target measurement was approximately  $1.66 \times 10^8$ , and  $1.11 \times 10^7$  for measurement with the carbon target. Fig. 2 displays the summing  $\Delta E - E_r$  scatter plot of the coincidence events over all the rings of downstream MRSD. In order to scrutinize the origin of non- $^9\text{Li}$  region events in Fig. 2, four typical regions were selected in which the ratios of events in coincidence spectrum to those in non-coincidence one were compared. It was found that the ratio in the  $^9\text{Li}$  region is much higher than those (nearly constant) in other three regions. We can thus conclude that the events in non- $^9\text{Li}$  regions result from the random coincidence caused by the noise tail in the proton spectrum of the upstream MRSD. The scatter plot of  $E_t$  vs.  $\theta_{\text{lab}}$  for the events within  $^9\text{Li}$  gate in Fig. 2 is shown in Fig. 3. The zone between two solid lines stands for the kinematics region of  $^9\text{Li}$  ground state, based on Monte Carlo simulation. This figure further demonstrates that the events within  $^9\text{Li}$  gate in Fig. 2 are the true  $^9\text{Li}$  products. Actually, the selection of  $^9\text{Li}$  events was individually performed for each ring of downstream MRSD. The energies and angles of protons on upstream MRSD relevant to the  $^9\text{Li}$  events appearing on the specific ring of downstream MRSD were restricted with the kinematics. Thus, the random coincidence events were effectively depressed by setting the corresponding windows for energies and angles (ring numbers) of protons. Finally about 50  $^9\text{Li}$  events were identified for the measurement with  $(\text{CD}_2)_n$  target and no background event was found in the same region for the carbon target run.

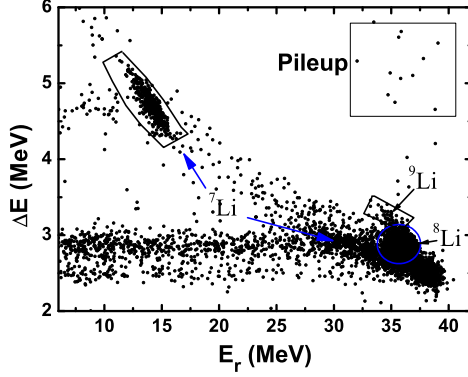


FIG. 2: Scatter plot of  $\Delta E$  vs.  $E_r$  for the  ${}^9\text{Li}$ -proton coincidence measurement with  $(\text{CD}_2)_n$  target. The 4 regions were selected to scrutinize the random coincidence events.

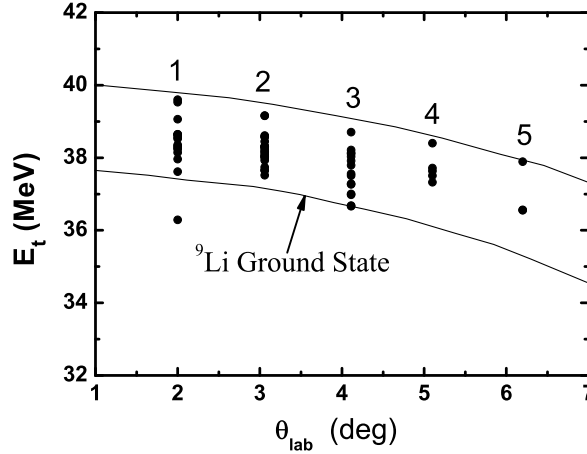


FIG. 3: Scatter plot of  $E_t$  vs.  $\theta_{\text{lab}}$  for the events within the  ${}^9\text{Li}$  gate in Fig. 2. The ring numbers of the downstream MASD are indicated.

Because of the existence of dead gaps in both MRSDs, a Monte Carlo simulation was used to calculate the coincidence efficiency between  ${}^9\text{Li}$  ions detected by downstream MRSD and protons by upstream one. The simulation took the geometrical factor, angular straggling and energy straggling into account. The coincidence efficiency was deduced from the ratio of the proton events in the relevant rings of upstream MRSD to the  ${}^9\text{Li}$  events in the specific ring of the downstream one. The differential cross sections can then be deduced. The resultant angular distribution is shown in Fig. 4. The uncertainties of differential cross sections mainly arise from the statistics and the assignment of  ${}^9\text{Li}$  gate; the angular uncertainties are from the angular divergence of  ${}^8\text{Li}$  beam, the finite size of beam spot, the angular straggling in the target and  $\Delta E$  detector as well as the width of each ring of the downstream MRSD.

The spin and parity of  ${}^8\text{Li}$  and  ${}^9\text{Li}$  (ground state) are  $2^+$  and  $3/2^-$ , respectively. The  ${}^8\text{Li}(d,p){}^9\text{Li}_{\text{g.s.}}$  cross section involves two components corresponding to ( $l = 1, j = 3/2$ ) and ( $l = 1, j = 1/2$ ) transfers, the differential cross section can be expressed as

$$\left(\frac{d\sigma}{d\Omega}\right)_{\text{exp}} = S_d[S_{1,3/2}\sigma_{1,3/2}(\theta) + S_{1,1/2}\sigma_{1,1/2}(\theta)], \quad (1)$$

where  $\left(\frac{d\sigma}{d\Omega}\right)_{\text{exp}}$  and  $\sigma_{l,j}(\theta)$  denote the measured and DWBA differential cross sections respectively,  $S_{1,3/2}$  and  $S_{1,1/2}$  are spectroscopic factors for the ground state of  ${}^9\text{Li} = {}^8\text{Li} \otimes n$ , corresponding to the  $j = 3/2$  and  $1/2$  orbits.  $S_d$  is the spectroscopic factor of deuteron that is close to unity. The  $S_{1,3/2}$  and  $S_{1,1/2}$  can be extracted by normalizing DWBA differential cross sections to the experimental data.

The finite-range DWBA code PTOLEMY [19] was used to compute the angular distribution. In the calculation, only the neutron transfer to the  $1p3/2$  orbit was taken into account because the contribution of the  $1p1/2$  orbit is less than 5% [16, 20]. All the entrance channel parameters were taken from Ref. [21], the exit channel ones from Refs. [21] and [22], respectively. Fig. 4 presents the normalized angular distributions for four sets of optical potential parameters, each curve corresponds to one spectroscopic factor,  $S_{1,3/2}$ . The average value of these spectroscopic factors was found to be  $0.68 \pm 0.14$  with the ‘‘standard’’ bound state potential parameters (radius  $r_0 = 1.25$  fm, diffuseness  $a = 0.65$  fm), it fairly agrees with the result  $S_{1,3/2} = 0.73$  extracted from the mirror reaction  ${}^8\text{B}(d,n){}^9\text{C}$  [20]. The cross section for the  ${}^8\text{Li}(d,p){}^9\text{Li}_{\text{g.s.}}$  reaction at  $E_{\text{c.m.}} = 7.8$  MeV was determined to be  $7.9 \pm 2.0$  mb through integration of the calculated angular distributions. The uncertainties of the spectroscopic factor and cross section result mainly from the difference of the optical potentials used in the calculation, as well as the statistical error of the measurement.

The  ${}^8\text{Li}(n,\gamma){}^9\text{Li}_{\text{g.s.}}$  cross section was calculated by assuming that the reaction proceeds by direct E1 capture of neutron to the ground state of  ${}^9\text{Li}$ . At low energies of astrophysical interest, the contribution of  $d$ -wave is negligible, the capture reaction is almost totally determined by the  $s$ -wave neutron capture process. The cross section for E1 capture of neutron to the ground state of  ${}^9\text{Li}$  with the orbital and total angular momenta  $l_f$  and  $j_f$  is given by

$$\sigma_{(n,\gamma)} = \frac{16\pi}{9} \left(\frac{E_\gamma}{\hbar c}\right)^3 \frac{e_{\text{eff}}^2}{k^2} \frac{1}{\hbar v} \frac{(2j_f + 1)}{(2I_1 + 1)(2I_2 + 1)} S_{l_f j_f} \times \left| \int_0^\infty r^2 w_{l_i}(kr) u_{l_f}(r) dr \right|^2, \quad (2)$$

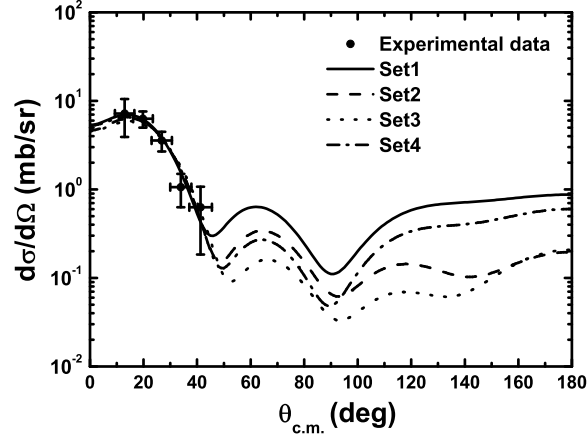


FIG. 4: Measured angular distribution of  ${}^8\text{Li}(d, p){}^9\text{Li}_{g.s.}$  at  $E_{c.m.} = 7.8$  MeV, together with DWBA calculations using different optical potential parameters.

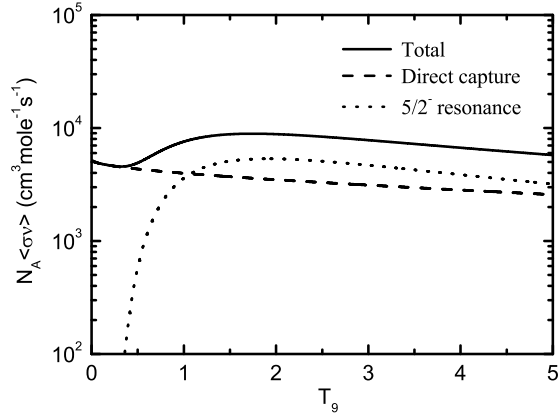


FIG. 5: Temperature dependence of the reaction rates for  ${}^8\text{Li}(n, \gamma){}^9\text{Li}$ . The contribution of direct capture is the result of present work and that of  $5/2^-$  resonance is taken from of Ref. [6].

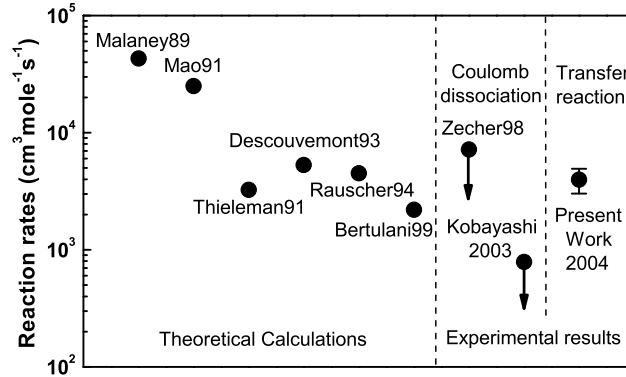


FIG. 6: The  ${}^8\text{Li}(n, \gamma){}^9\text{Li}$  reaction rates for the direct capture derived from theoretical calculations and experiments.

where  $E_\gamma$  stands for the  $\gamma$ -ray energy,  $v$  is the relative velocity between particles 1 (neutron) and 2 ( $^8\text{Li}$ ),  $k$  the incident wave number,  $I_i$  the spin of particle  $i$ .  $e_{\text{eff}} = -eZ/(A+1)$  is the neutron effective charge for the E1 transition in the potential produced by a target nucleus with mass number  $A$  and atomic number  $Z$ .  $w_{l_i}(kr)$  is the distorted radial wave function for the entrance channel,  $u_{l_f}(r)$  the radial wave function of the bound state neutron in  $^9\text{Li}$  which can be calculated by solving the respective Schrödinger equation. The optical potential for the neutron scattering on unstable nucleus  $^8\text{Li}$  is unknown experimentally. We adopted a real folding potential which was calculated using the  $^8\text{Li}$  density distribution from the measured interaction cross section [23] and an effective nucleon-nucleon interaction DDM3Y [24]. The imaginary part of the potential is very small because of the small flux into other reaction channels and can be neglected in most cases involving neutron capture reaction. The depth of the real potential was scaled to  $J_V/A = 743 \text{ MeV fm}^3$ , the volume integral of potential per nucleon. Usually, the optical potential changes considerably for different nuclei, whereas the volume integral of potential per nucleon is a more stable quantity relatively. First, we calculated the folding potentials for  $^6,7\text{Li}$  and  $^{12}\text{C}$ , whose neutron capture cross sections were measured [25, 26, 27], and found  $J_V/A = 749 \pm 23$ ,  $729 \pm 75$  and  $742 \pm 12 \text{ MeV fm}^3$ , respectively, by fitting to the experimental cross sections. One can see that these values are close to each other, indicating the stability of the potential volume integral. Then the weighted average of above values was taken as the  $J_V/A$  value for  $^8\text{Li}$ . As soon as the potential is known, the capture cross sections can be calculated with the Eq. (2). With the spectroscopic factor extracted from the present experiment, the energy dependence of direct capture cross sections for the  $^8\text{Li}(n, \gamma)^9\text{Li}_{\text{g.s.}}$  reaction were calculated, showing a deviation from the usual  $1/v$  behavior. Fig. 5 demonstrates the temperature dependence of the reaction rate for the direct capture in  $^8\text{Li}(n, \gamma)^9\text{Li}$  together with that for the resonant capture at  $5/2^-$  4.3 MeV state in  $^9\text{Li}$  (deduced by Rauscher et al. [6] with  $\Gamma_\gamma = 0.65 \text{ eV}$  and  $\Gamma_{\text{tot}} = 100 \text{ keV}$ ), as well as the total reaction rate. Direct capture to the first excited state at 2.69 MeV is not include in the calculation since the transition strength is believed to be negligible [13, 14]. It can clearly be seen that the direct capture plays an important role in the  $^8\text{Li}(n, \gamma)^9\text{Li}$  reaction especially in the astrophysical environment of  $T_9 < 1$ . The reaction rate for the direct capture was found to be  $N_A \langle \sigma v \rangle = 3970 \pm 950 \text{ cm}^3 \text{mole}^{-1} \text{s}^{-1}$  at  $T_9 = 1$ , the uncertainty arises from the errors of spectroscopic factor and the volume integral of potential per nucleon. The  $^8\text{Li}(n, \gamma)^9\text{Li}$  reaction rates for the direct capture derived from

theoretical calculations and experiments are shown in Fig. 6, our result is significantly higher than the upper limit from the most recent Coulomb dissociation experiment [13] and approximately in agreement with the theoretical estimations reported in Refs. [6, 10].

In summary, we have measured the angular distribution of the  ${}^8\text{Li}(d, p){}^9\text{Li}_{\text{g.s.}}$  reaction at  $E_{\text{c.m.}} = 7.8$  MeV, through coincidence detection of  ${}^9\text{Li}$  and recoil proton, and obtained the cross section. By using the spectroscopic factor deduced from the  ${}^8\text{Li}(d, p){}^9\text{Li}_{\text{g.s.}}$  angular distribution, we have successfully derived the  ${}^8\text{Li}(n, \gamma){}^9\text{Li}_{\text{g.s.}}$  direct capture cross section and astrophysical reaction rate for the first time.

This work was supported by the Major State Basic Research Development Program under Grant Nos. G200077400 and 2003CB716704, the National Natural Science Foundation of China under Grant Nos. 10375096, 10025524 and 19935030.

- 
- [1] M. Terasawa, K. Sumiyoshi, T. Kajino, G. J. Mathews, and I. Tanihata, *Astrophys. J.* **562**, 470 (2001).
  - [2] T. Kajino, S. Wanajo, and G. J. Mathews, *Nucl. Phys. A* **704**, 165c (2002).
  - [3] S. Rosswog, C. Freiburghaus, and F. K. Thielemann, *Nucl. Phys. A* **688**, 344c (2001).
  - [4] T. Kajino and R. N. Boyd, *Astrophys. J.* **359**, 267 (1990).
  - [5] N. Hata, R. J. Scherrer, G. Steigman, D. Thomas, T. P. Walker, S. Bludman, and P. Langacker, *Phys. Rev. Lett.* **75**, 3977 (1995).
  - [6] T. Rauscher, J. H. Applegate, J. J. Cowan, F.-K. Thielemann, and M. Wiescher, *Astrophys. J.* **429**, 499 (1994).
  - [7] H. Miyatake, H. Ishiyama, M.-H. Tanaka, Y. X. Watanabe, N. Yoshikawa, S. C. Jeong, Y. Matsuyama, Y. Fuchi, T. Nomura, T. Hashimoto, et al., *Nucl. Phys. A* **738**, 401 (2004).
  - [8] R. A. Malaney and W. A. Fowler, *Astrophys. J.* **345**, L5 (1989).
  - [9] Z. Q. Mao and A. E. Champagne, *Nucl. Phys. A* **522**, 568 (1991).
  - [10] K. K-Thieleman, J. H. Cowan, and M. Wiescher, *Nuclei in the Cosmos*, ed. H. Oberhummer et al. (1991), (Berlin:Springer).
  - [11] P. Descouvemont, *Astrophys. J. Lett.* **405**, 518 (1993).
  - [12] C. A. Bertulani, *J. Phys. G* **25**, 1959 (1999).

- [13] H. Kobayashi, K. Ieki, Á. Horváth, A. Galonsky, N. Carlin, F. Deák, T. Gomi, V. Guimaraes, Y. Higurashi, Y. Iwata, et al., *Phys. Rev. C* **67**, 015806 (2003).
- [14] P. D. Zecher, A. Galonsky, S. J. Gaff, J. J. Kruse, G. Kunde, E. Tryggestad, J. Wang, R. E. Warner, D. J. Morrissey, K. Ieki, et al., *Phys. Rev. C* **57**, 959 (1998).
- [15] C. Rolfs, *Nucl. Phys. A* **217**, 29 (1973).
- [16] P. Mohr, *Phys. Rev. C* **67**, 065802 (2003).
- [17] M. J. Balbes, M. M. Farrell, R. N. Boyd, X. Gu, M. Hencheck, J. D. Kalen, C. A. Mitchell, J. J. Kolata, K. Lamkin, R. Smith, et al., *Nucl. Phys. A* **584**, 315 (1995).
- [18] W. Liu, Z. Li, X. Bai, Y. Wang, G. Lian, S. Zeng, S. Yan, B. Wang, Z. Zhao, T. Zhang, et al., *Nucl. Instrum. Methods Phys. Res. B* **204**, 62 (2003).
- [19] M. H. Macfarlane and S. C. Pieper, *Argonne National Laboratory Report* (unpublished).
- [20] D. Beaumel, T. Kubo, T. Teranishi, H. Sakurai, S. Fortier, A. Mengoni, N. Aoi, N. Fukuda, M. Hirai, N. Imai, et al., *Phys. Lett. B* **514**, 226 (2001).
- [21] C. M. Perey and F. G. Perey, *Atomic data and nuclear data tables* **17**, 1 (1976).
- [22] B. A. Watson, P. P. Singh, and R. E. Segel, *Phys. Rev.* **182**, 977 (1969).
- [23] I. Tanihata, H. Hamagaki, O. Hashimoto, Y. Shida, N. Yoshikawa, K. Sugimoto, O. Yamakawa, T. Kobayashi, and N. Takahashi, *Phys. Rev. Lett.* **55**, 2676 (1985).
- [24] A. M. Kobos, B. A. Brown, R. Lindsay, and G. R. Satchler, *Nucl. Phys. A* **425**, 205 (1984).
- [25] T. Ohsaki, Y. Nagai, M. Igashira, T. Shima, H. Kitazawa, K. Takaoka, M. Kinoshita, Y. Nobuhara, A. Tomyo, H. Makii, et al., *AIP Conference Proceedings* **529(1)**, 458 (2000).
- [26] J. C. Blackmon, A. E. Champagne, J. K. Dickens, J. A. Harvey, M. A. Hofstee, S. Kopecky, D. C. Larson, D. C. Powell, S. Raman, and M. S. Smith, *Phys. Rev. C* **54**, 383 (1996).
- [27] Y. Nagai, M. Igashira, N. Mukai, T. Ohsaki, F. Uesawa, K. Takeda, T. Ando, H. Kitazawa, S. Kubono, and T. Fukuda, *Astrophys. J.* **381**, 444 (1991).